Cell Geometry Impact on the Cell Filling Process in Gravure Printing for Printed Electronics

Xiaoer Hu
Vivek Subramanian, Ed.
Tsu-Jae King Liu, Ed.

Electrical Engineering and Computer Sciences
University of California at Berkeley

Technical Report No. UCB/EECS-2018-165
http://www2.eecs.berkeley.edu/Pubs/TechRpts/2018/EECS-2018-165.html

December 10, 2018

Acknowledgement

I want to thank my advisors, Professor Vivek Subramanian and Professor Tsu-Jae King Liu, for their support, expertise and guidance. I am grateful to the Printed Electronics Group and my friends, for all of their support and suggestions.

To my parents and grandparents, thank you for all of your constant love, support, guidance, and encouragement throughout my life. To Guanglong, thank you for accompanying me through all the hard moments and good times in my graduate study and life.

Cell Geometry Impact on the Cell Filling Process in Gravure Printing for Printed Electronics

by Xiaoer Hu

Research Project

Submitted to the Department of Electrical Engineering and Computer Sciences, University of California at Berkeley, in partial satisfaction of the requirements for the degree of **Master of Science, Plan II**.

Approval for the Report and Comprehensive Examination:

Committee:

Vivek Subramanian

Professor Vivek Subramanian
Research Advisor

Dec 10, 2018

Date:

* * * * * * *

Professor Tsu-Jae King Liu
Second Reader

December 7, 2018

Date:

Abstract

Cell Geometry Impact on the Cell Filling Process in Gravure Printing for Printed Electronics

by

Xiaoer Hu

Master of Science in Electrical Engineering and Computer Sciences

University of California, Berkeley

Professor Vivek Subramanian, Chair

Highly scaled gravure printing has attracted great attention recently because of its high resolution, large throughput, and low cost. Cell filling is the first step in the actual gravure printing process, and it strongly determines the quality of printed patterns. Therefore, systematically studying the impact of cell geometry on the filling process is necessary to better understand and improve gravure printing. In this work, we demonstrate the fabrication details to make cells with different cross-section geometries, a novel setup that provides filling details for sub-5 μm cells in real-time to understand the geometry impacts on cell filling process, and a model that helps to predict the filling failure regimes. Cell filling fails when the ink cannot replace air inside the cells completely, because this may result in discontinuous lines and non-uniform films in printed patterns. By varying the viscosity and flow speed of the fluid, we conclude that the dimensionless capillary number is a good indicator for this cell filling study. Cell filling fails for round shape and pyramid shape cells at high capillary numbers, and a unique "advancing filling" phenomenon occurs for round shape cells at low capillary numbers. The round shape cells can be filled at higher capillary numbers than pyramid shape cells, so this type of cell geometry can potentially be applied in future gravure printing master designs. Square shape cells are difficult to be filled, even at small capillary numbers, and therefore should not be used in gravure printing.

Acknowledgements

I would like to express my sincere gratitude to my advisor, Professor Vivek Subramanian, for his continuous support of my Master study and related research. His patience, motivation, and knowledge strengthened my ability to think and study independently as a graduate student.

I would like to thank my PhD advisor, Professor Tsu-Jae King Liu, for giving me feedback and taking the time to read this report. Her patience, expertise, and guidance helped me to become a better graduate student and continue my research in the field of electrical engineering.

Additionally, I would like to thank the entire Printed Electronics Group at Berkeley. I want to thank Jake Sporrer for training me on gravure printers and providing useful discussions both theoretically and experimentally. I thank Alvin Li for giving me useful suggestions on the model building. I want to acknowledge Raj Kumar for revising this report and providing me with useful writing tips. I am grateful to Matt McPhail and Carlos Biaou for their help in both the lab techniques and general research findings useful for my project. I appreciate the help from Nishita Deka and Steve Volkman on the silicon master fabrication. In particular, I want to thank the previous students in our group, Gerd Grau, Artos Cen, and Will Scheideler for answering my questions on gravure printing and the cell filling experiments.

I would also like to sincerely thank my friend Xiaosheng Zhang, for helping me build the experimental setup and discussing the filling mechanisms with me. My friends, Jason Wu and Yichi Zhang, were extremely kind, supportive, and helpful in leading me to the amazing world of nanofabrication.

Finally, I especially would like to thank my parents and grandparents, for all of their constant love, support, guidance, and encouragement throughout my life. They always encouraged me to follow my passion, chase my dream, and become the person that I want to be. I want to also thank Guanglong Huang for accompanying me through all the hard moments and good times in my graduate study and life.

Table of Contents

Chapter 1: Introduction

1.1 Background

Printing technologies for the fabrication of electronic devices have received significant interest in recent years because they can be applied to fabricate electronic devices on flexible substrates with low-cost and large-area[1,2]. For example, flexible displays, organic photovoltaic devices, and printed RFID tags can all be developed using printing technologies[3-6]. Among the various available printing technologies, highly scaled gravure printing overcomes the traditional tradeoff between printing speed and resolution patterning. Gravure printing can achieve printing speeds above 1 m/s with feature sizes below 5 μm[7].

Gravure printing includes four sub-processes, as described in Figure 1[7,8]. First, the ink needs to fill in the cells, and ideally cells should be filled by ink without any air entrapment to maximize the ink within the individual cells. Then the excess ink is wiped by a doctor blade. Ideally, there is no additional ink outside of the cells and the cells are still fully filled with ink. After wiping, all the ink is removed from the cells and transferred onto the substrate. Last, the ink on the substrate is spread to fill in the gaps in between the individual cells and form the desired patterns.

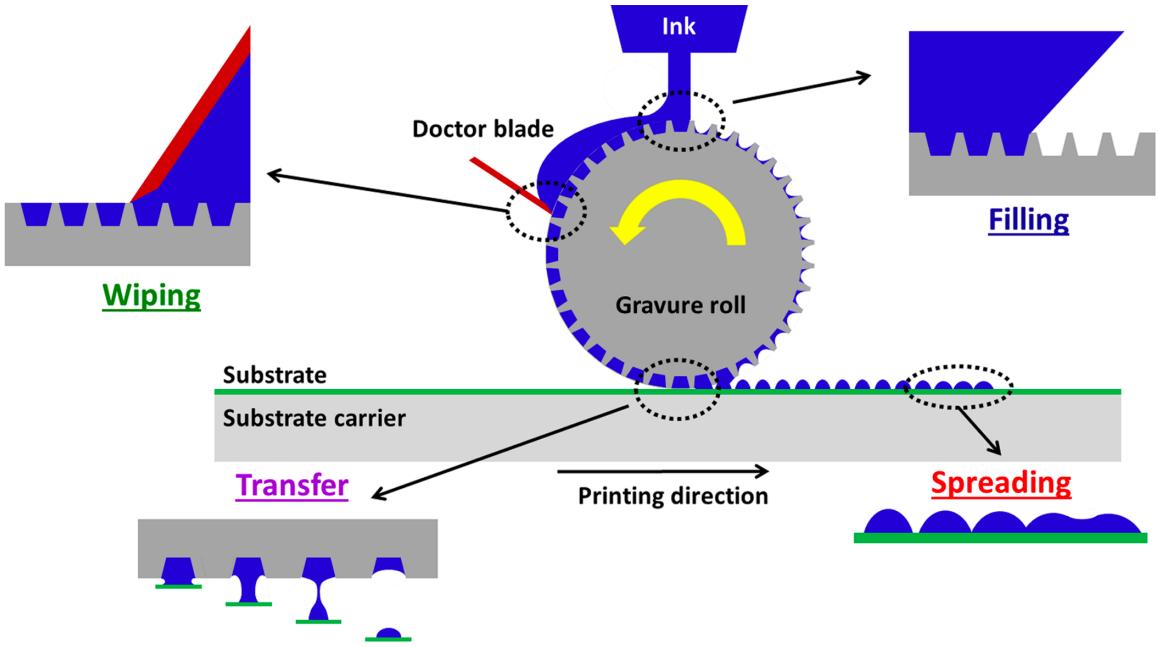

Figure 1: The overview of gravure printing and its four sub-processes: cell filling, doctor blade wiping, ink transfer, and ink spreading on the substrate[7]. Copyright 2016 American Chemical Society.

For industrial-scale gravure printing, cells are always created by electromechanical engraving or laser patterning[9,10]. However, these traditional engraving techniques cannot achieve less than 10 μm cell size. Furthermore, these techniques increase non-ideality of the cell shapes and have less controllable cell cross-sections, which can lead to partial filling of cells, discontinuous printed features, or other defects that hinder device performance[11,12].

1.2 Motivations of the Cell Filling Study

The cell filling process in gravure printing is related to how a fluid contact line moves on engraved surfaces, and how the air-liquid interface deforms into or over the engraved cells. Few reports to date have focused on the cell filling process. Previous works have primarily studied the two-dimensional filling cases for simple grooves at the

macroscale[13,14], or focused on low capillary number situations[8]. There is one paper discussing the cell filling for gravure printing at different capillary numbers for different cell sizes, also from our previous work[12]. In that work, we chose photolithography and KOH anisotropic wet etch to fabricate cells with pyramid shapes on a (100) silicon wafer, and focused on the cell filling by silicone oil at different speeds. The previous results show that the filling is strongly dependent on the capillary number, and fails at high capillary number because of air bubble entrapment inside the cells. Moreover, by comparing the filling for cells from 30 μm to 100 μm, the previous work concluded that the filling does not depend on the cell size, although images for cells smaller than 40 μm are not clear enough due to the optical resolution limits.

Therefore, although filling for simple two-dimensional cases and for three-dimensional pyramid shape cells have been studied, a systematic study for cells with different cross-section geometries and sub-5 μm sizes is needed to better understand the filling process in gravure printing, and to help push highly scaled gravure printing to higher speeds and smaller feature sizes. In this work, we report new methods to fabricate cells with different cross-section geometries, and a novel setup that enables direct observation of the cell filling process at different capillary numbers for 5 μm cells in real time. In addition, the impact of capillary number and cell geometry on cell filling is modeled to help predict the situation for incomplete filling and guide future gravure cell designs.

Chapter 2: Experimental Section

2.1 Fabrication Process of Gravure Printing Master

Since the roll curvature has a negligible impact on the filling process, both direct (using a gravure cylindrical roll as the printing master) and indirect (using a flat surface as the printing master) gravure printing should give the same results for cell filling[12]. Observing the filling for direct printing in real time is difficult, so the indirect printing process is chosen in this work. The flat gravure master is made using a (100) Si wafer. Arrays of microscale cells with square-shaped top view but different cross-section shapes are fabricated using standard photolithography and different etching methods.

In order to make a gravure master with pyramid shape cross-section cells, 1 μm thick thermal oxide is grown on the Si wafer by wet oxidation, and photolithography process creates a mask for oxide etch. The oxide is etched by reactive ion etching using CF_4 and CHF_3 with about 20% over-etch, and is patterned with steep sidewall angles. After striping the photoresist, KOH solution with 24% by volume at 80 °C etches the Si openings with a perfect inclination angle of 54.7°. Finally, the oxide mask is stripped by dipping the wafer in 5:1 BHF solution for 12 minutes, and the Si wafer can be applied to perform gravure printing as a printing master. The etching time in KOH can be varied to obtain different cross-sections.

Similarly, the wafers with square shape cells can be fabricated by coating photoresist on Si wafer, performing standard photolithography process, etching Si anisotropically by inductively coupled plasma with bias using Cl_2 and HBr for 5 to 8 minutes with etch rate about 0.2 μm/s, and striping the photoresist. The etching differences between round and

square shape cells are: after photolithography, the Si wafer with round shape cross-section cells is dipped in 10:1 HF solution for 15 minutes to remove the native oxide, and etched by XeF_2. The cross-sections of the above three types of cells are shown in Figure 2. The depths of square and round shape cross-section cells are chosen to maintain the same cell volumes that the pyramid shape cells have.

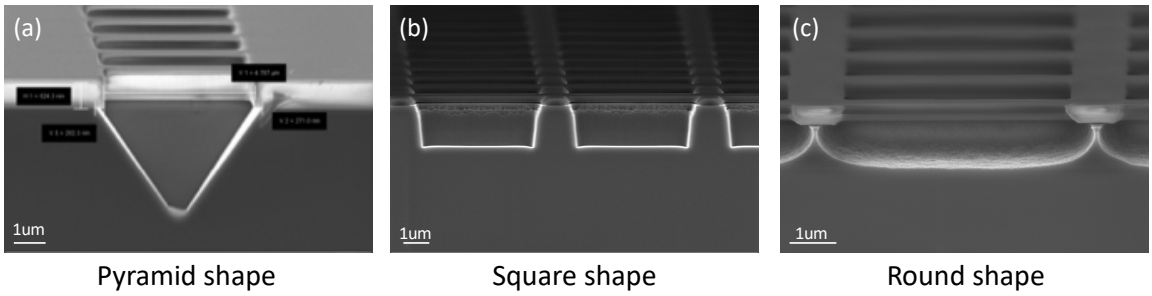

Figure 2. The SEM image of cross-section of (a) pyramid shape cell (b) square shape cell, and (c) round shape cell.

The cell opening width on all the wafers are from 1 μm to 8 μm with a discretized step 1 μm, and 5 μm cells are studied because previous work has shown that in microscale, the cell sizes do not impact whether the cells can be completely filled[12]. The etching methods can be modified in the future to make more types of cross-sections for cell filling study. For instance, we can use HNA to isotropically wet etch the round shape cross-section cells, or use other dry etch gases such as SF_6, C_4F_8, and O_2 to tune the sidewall geometries. Note that all of these cell geometries can then be used as master molds to produce gravure rolls, as we have described in our previous work[11].

2.2 Experimental Setup

Figure 3 shows the experimental setup. The printing master is put on a linear stage under a long working distance objective lens with 100x magnification. On top of the lens, we

include a high-speed camera to capture cell filling on the Si wafer at 200 frames per second. Silicone oil is selected as the ink for filling study because it is easy to clean, has a wide range of viscosities that provide us tunable capillary numbers, and solidifies slowly. Silicone oil is a Newtonian liquid, and future work can be done for non-Newtonian liquids to obtain a better understanding of filling in more realistic and complex cases. Then ~50 μL silicone oil is injected on the Si wafer. A plastic squeegee with 3 cm header pushes the ink to move forward at any desired speed, and the cell filling can be observed directly from the objective lens and camera. By moving the linear stage beneath the Si wafer, this process can be repeated to fill the cells at different speeds, until the entire wafer is covered by the ink. Filling by silicone oil with different viscosities is also studied for cells with different cross-section shapes. Therefore, the cell filling process can be visualized in real time using different capillary numbers. After the experiments, the wafers are cleaned by spraying toluene on the surface and are sonicated in toluene for 15 minutes. The cleaned structures can then be reused for subsequent experiments.

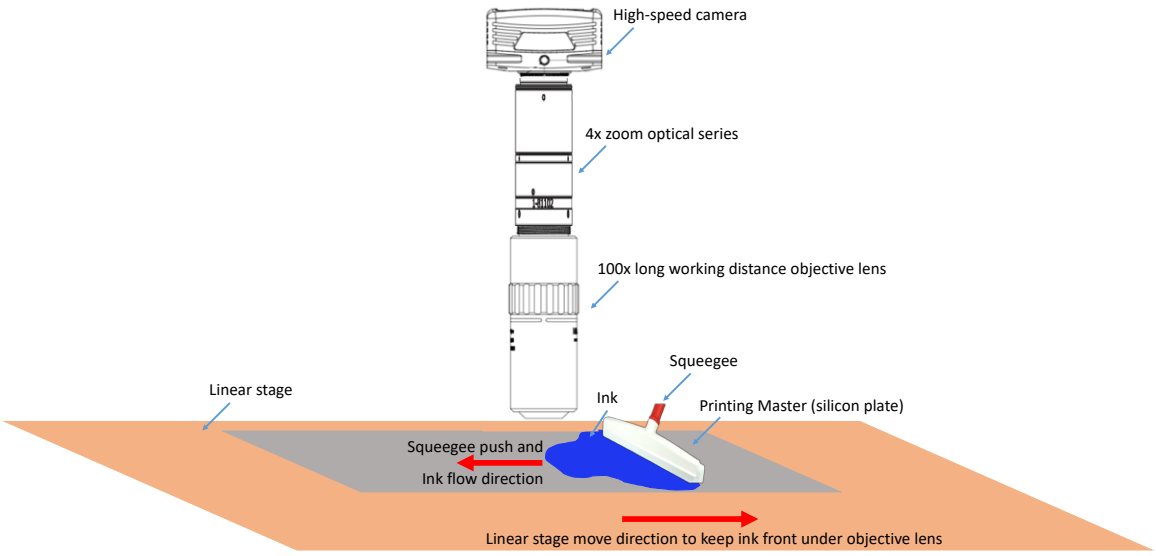

Figure 3. Schematic plot of the experimental setup.

Chapter 3: Results and Discussion

3.1 Qualitative Analysis

In the cell filling process, the overall liquid contact line moves at the printing speed, and the speed that the fluid enters the cell is determined by the combination of viscous forces and surface tension. The contact line here refers to the front of the fluid. The viscous force acts as a resistance force for fluids to flow, while the surface tension is the driving force for flows at the microscale. Therefore, the speed of the fluid entering the cell is proportional to surface tension divided by viscosity of the fluid. Filling fails when the contact line outside of the cell reaches the back edge of the cell, while the volume of the fluid entering the cell is much smaller than the cell volume. Therefore, we define a dimensionless parameter called capillary number, which relates the viscous force, surface tension force, and printing speed as:

$$Ca = \frac{U\mu}{\gamma} \qquad \textit{Equation 1}$$

where U is the printing speed, or the contact line moving speed outside of the cell, μ is the viscosity of the fluid, and γ is the surface tension of the fluid.

We perform the filling for cells with different cross-section shapes at the same ink viscosity and printing speed, to qualitatively analyze the cell geometry impact. Figure 4 shows the cell filling over time for different cell shapes. The silicone oil flows from right to left, its viscosity is 10 kcSt, and the capillary number is 0.5. For all cell shapes studied, the center contact line pins at the front edge of the cell at first, while the side contact lines move freely outside of the cell. After a certain amount of time, the center contact line

releases and starts to move into the cells to replace the air inside the cell, whilst the side contact lines reach the back edge.

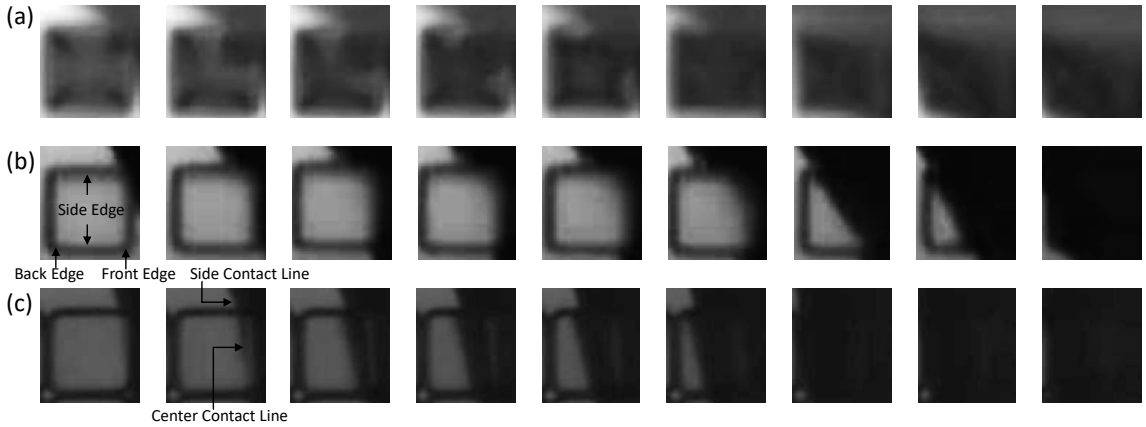

Figure 4. The cell filling process of 5 μm cells using the same capillary number at roughly the same times (top view). The cell cross-section geometries are: (a) pyramid shape, (b) square shape, and (c) round shape. The fluid flows from right to left, and the time increases from the leftmost picture to the rightmost picture.

Filling for pyramid cells starts from the cell wedge instead of the cell face, and the liquid fills from the bottom tip to the top surface, then the overall fluid covers the entire cell. The filling will be completed if the liquid can replace all the air inside the cell before the cell is covered by the overall fluid front. From the previous study, when the capillary number ranges from 0.1 to 1.0, the cell filling for pyramid shape cells is at the transition point between "completely filled" and "non-filled"[12]. The square cross-section cells, however, are the most difficult to be filled, because the center contact line remains pinned at the front edge while the side contact lines travel along the cell side edges. When the side contact lines almost reach the back edge, the overall fluid starts to fill/cover the cell, and we will prove later that this is indeed covering instead of filling, although directly from the pictures, there are no differences between filling and covering, due to the optical limit of the high magnification objective lens. For the round cross-section cells, filling is easy, because after

the center contact line pins at the front edge for a small amount of time, the center contact line travels faster than the side contact lines, which means filling of this type of cell is very easy compared with the other two types of cell geometries. Therefore, from the qualitative comparisons, the easiest cell geometry for cell filling is the round shape, and the most difficult filling geometry is the square shape.

3.2 Quantitative Analysis

3.2.1 Methods

To quantitatively analyze the data, we apply MATLAB to binarize the pictures during filling for round shape and square shape cross-section cells. We treat the area covered by ink, as well as the cell boundaries as "0" (black), and other areas as "1" (white), as shown in Figure 5. Inside the cell boundaries, the number of white area pixels at each time can be calculated, and this represents the unfilled area. The unfilled area before the center contact line reaches the cell is the total area of the cell, and therefore we calculate the filled area A_f as the total area minus the unfilled area at each time. The percent of filled area, A_f^*, is defined as filled area divided by total area. We also find the side contact line front from the binarized pictures, and track its movement during the filling process. The inner right boundary is defined as "zero" travel distance for the side contact line front, the cell's right side is treated as "negative" travel distance, and the left side has "positive" travel distance relative to the cell itself. Therefore, after finding the number of pixels between the contact line front and the inner right boundary, the travel distance of the ink front can be derived. Combining the SEM cross-section images and the cell boundaries in the binary pictures, the relationship between one pixel and real-life dimensions can be established for all types

of cells, and the side contact line travel distance, D_c, can be extracted from the pictures. Since the cell opening lengths are slightly different for cells with different cross-sections, we define relative contact line travel distance, D_c*, instead, and it is defined as the ratio of side contact line travel distance to the cell opening length.

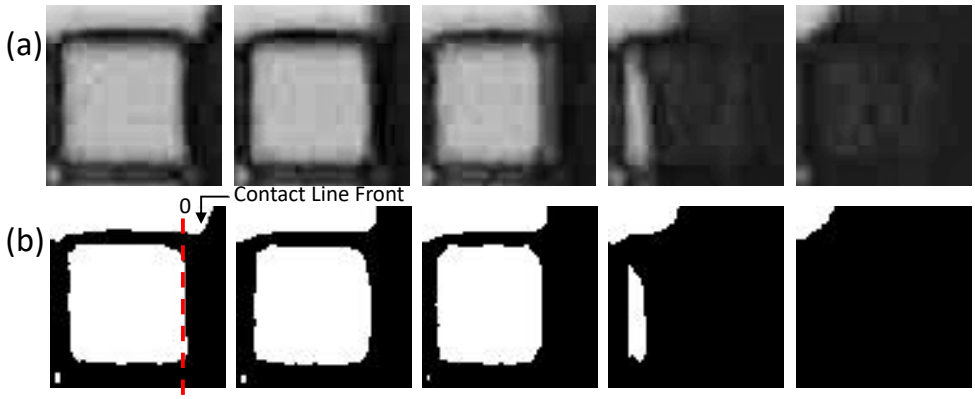

Figure 5. An example of (a) original pictures and (b) its corresponding binary pictures (top view). This figure shows the filling process of round shape cross-section cells when capillary number is 0.15. The fluid flows from right to left, and the time increases from the leftmost picture to the rightmost picture.

3.2.2 Analysis

We apply this model to plot relationships between A_f*, percent of filled area, and D_c*, relative contact line front travel distance, for round shape cells with the same viscosity but different printing speeds, and different viscosities but the similar capillary numbers, as shown in Figure 6(a) and (b). First, all the curves have similar slopes, and this slope reflects the filling progress as side contact line moves. When capillary number increases, the curve shifts to the right, indicating that filling becomes more difficult, as shown in Figure 6(a). Filling will fail when the side contact line front reaches the back edge while the fluid does not replace a large portion of air inside the cell. In other words, cell filling fails when $D_c^* \approx 1$ and $A_f^* \approx 0$, which happens at high capillary numbers for this type of cell geometry.

Furthermore, Figure 6(a) additionally suggests that capillary number is a good dimensionless indicator for cell filling studies, consistent with previous work, because the curves of fluids with different viscosities, different printing speeds, but similar capillary numbers overlap with each other, meaning the filling behavior of the round shape cross-section cells depends on the dimensionless capillary number.

Moreover, from Figure 6(b), when capillary number is very small, for example, 0.02, the curve shifts to strongly left, and $A_f^* \approx 1$ when $D_c^* < 0$ (in this case, $A_f^* \approx 1$ when $D_c^* \approx -1$). Three filling pictures for round shape cross-section cells at low capillary number are shown in Figure 6(c), which imply that there are three different filling stages in this case, and the center contact line moves even faster than the side contact line. This fast travel of center contact line causes the A_f* vs. D_c* curve at Ca = 0.02 in Figure 6(b) to shift to the far left. At stage 1, filling of the studied cell happens, while its previous cell is also experiencing filling and the previous cell is closer to the side contact line. Therefore, the filling speed of the studied cell slows down, and the slope of the A_f* vs. D_c* curve is smaller. Once the previous cell is fully filled and its next cell is totally empty, filling enters to the second stage. In the third stage, the next cell starts to get a small amount of fluid. Therefore, the filling speed of the studied cell becomes closer to the number at higher capillary numbers, and the slope goes back to the slope that other curves have, in both stage 2 and stage 3. This "advancing filling" phenomenon only occurs for round shape cross-section cases at low capillary numbers, which also indicates that round shape cross-section cells are easier to be filled than pyramid shape and square shape cells.

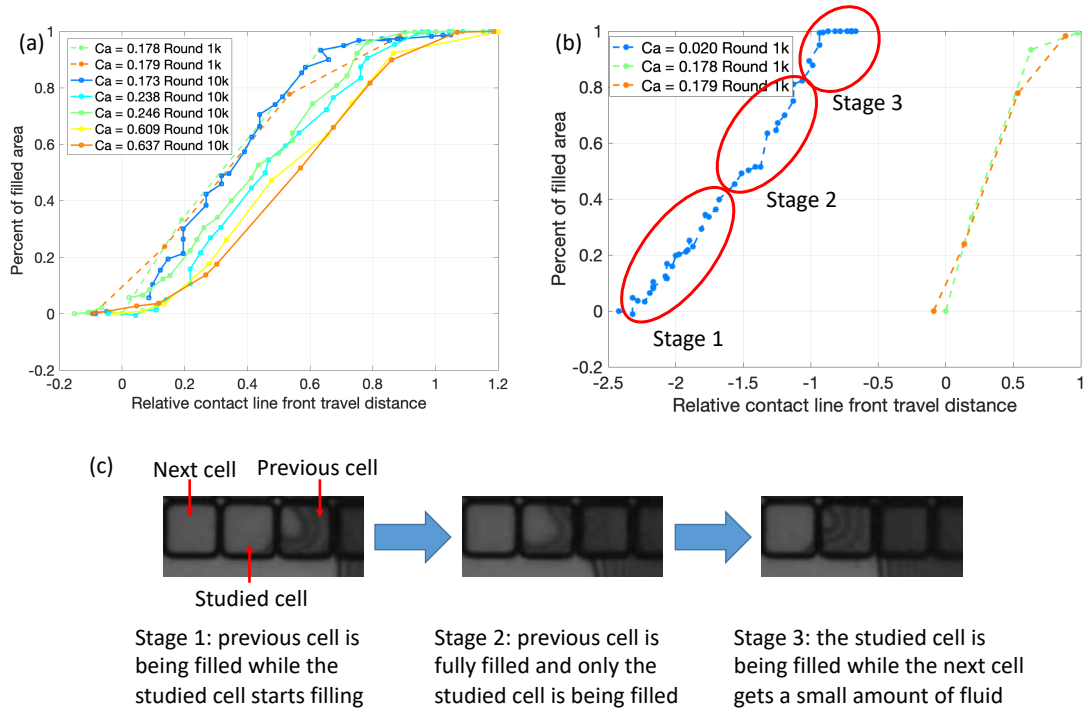

Figure 6. Percent filled area A_f* vs. relative contact line front travel distance D_c* plot for round shape cross-section cells. (a) Curves with the same viscosity (10 kcSt in solid lines and 1 kcSt in dashed lines) but different printing speeds, and the same capillary number (~0.17) but different viscosities; (b) Curves with the same viscosity (1 kcSt) but different speeds (low or moderate capillary numbers). (c) The three stages of cell filling process when capillary number is 0.02 (top view).

The same experiment is also done for square shape cross-section cells, and the results are shown in Figure 7(a). For all the curves, $A_f^* \approx 0$ while D_c^* increases and approaches 1. This relationship means the center contact line only enters the cell from the front edge slightly, while the side contact lines move along the side edges, almost arrive at the back edge, and trap the air. Therefore, it is impossible for the fluid to replace the air inside the square shape cells, and the plausible "filling" seen from the pictures is actually because the fluid covers the top of the cell. This non-filled situation can also be verified by all the curves with the same viscosity but different printing speeds. Unlike the shifting trend in

Figure 6, Figure 7(a) shows that for square shape cross-section cells, larger speeds correspond to left shift of the curves. Since the fluid only covers the top of the cell, the covering speed depends on the printing speed, and larger printing speed results in faster covering. In addition, the curves for square shape cells do not significantly depend on the viscosity of the fluid, which means the viscous force does not play an important inhibiting role in this process, and therefore filling does not happen. The difficulty of filling square shape cross-section cells is that the driving force for filling is the surface tension force, which only happens when the contact angle between the fluid and the solid surface is larger than the advancing contact angle. Since the sidewall of square shape cells is about 90°, when the center contact line of the fluid moves to the cell front edge, the contact angle reduces by 90° suddenly, pinning the contact line at the front edge, as shown in Figure 7(b). The center contact line will stay pinned unless the contact angle exceeds the advancing contact angle again. At the same time, the side contact line still moves at the printing speed towards the back edge, resulting in air entrapment in the cell. Bankoff[14] theoretically analyzes entrapment of air during fluid spreading in two-dimensional grooves. Although this analysis focuses on millimeter scale rough surface, the results show that when sidewall angle φ and the liquid contact angle θ have the relationship: $\theta > 180° - 2\varphi$, there is always gas entrapment in the two-dimensional grooves that cannot be replaced by the liquid. Bankoff also shows that if the groove has semicircular cross-section, it is impossible to trap the gas as long as the arc is less than a semi-sphere. Our experimental results verify that in the microscale, three-dimensional case, filling is still impossible for cells with large sidewall angles, and very easy for cells with round cross-section shapes. Therefore, square shape cross-section cells are not good choices for gravure printing in terms of cell filling.

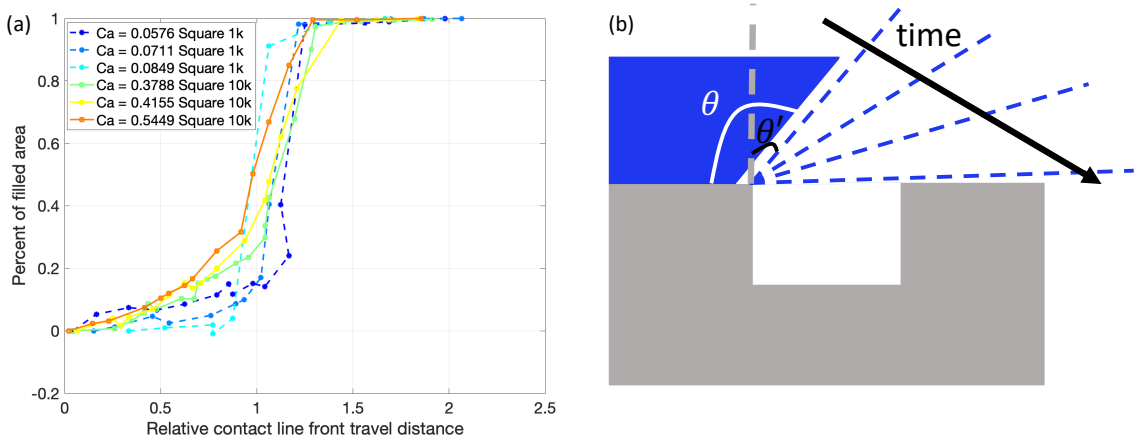

Figure 7. (a) Percent filled area A_f* vs. relative contact line front travel distance D_c* plot for square shape cross-section cells. Solid lines represent fluid with 10 kcSt viscosity and dashed lines correspond to 1 kcSt viscosity fluid. (b) Cross-sectional schematic plot of center contact line pinning phenomenon for square shape cross-section cells. The contact angle is labelled as θ before the fluid reaches the cell edge, and is labelled as θ′ when the fluid starts being pinned at the edge.

For pyramid shape cells, our previous work shows that the transition point between completely filled and non-filled falls between Ca = 0.1 and 1.0. That is, partial filling happens when capillary number is in this range. The model for this case is more complex and different from that for square and round shape cells.

Therefore, the cells with round shape cross-section are the easiest to be filled compared with pyramid shape and square shape cells, and they have the unique "advancing filling" phenomenon under low capillary numbers. The pyramid shape cells can also be filled, but the upper bound of capillary number for filling is 1, and partial filling happens when capillary number is larger than 0.1. The square shape cells, however, are almost impossible to be filled in real printing scenarios, and therefore are not suitable for gravure printing in terms of cell filling.

Chapter 4: Summary and Conclusion

We demonstrate the fabrication details to make cells with different cross-sections for highly scaled gravure printing, and systematically study the cell geometry impact on cell filling process using a novel experimental setup that allows us to observe the filling details of cells with sub-5 μm openings. After analyzing the pictures by our model, the cells with round shape cross-section are found to be the easiest for filling, and their filling depends on capillary number. At low capillary numbers, “advancing filling” happens. Higher capillary numbers result in more difficult filling. If the center contact line cannot replace the air inside the cell completely before the side contact lines reach the back edge, air bubbles will be entrapped in the cell, causing filling failure. The square shape cross-section cells are hard to be filled due to their large sidewall angles, and therefore this geometry should not be selected for gravure printing masters. Future work can be done to study the ink transfer process for different cell geometries, or focus on non-Newtonian fluids. Moreover, the surface roughness may also impact cell filling, and this can be tuned by coating the cell surface with different materials.

References

(1) Subramanian, V.; Chang, J. B.; de la Fuente Vornbrock, A.; Huang, D. C.; Jagannathan, L.; Liao, F.; Mattis, B.; Molesa, S.; Redinger, D. R.; Soltman, D.; et al. Printed Electronics for Low-Cost Electronic Systems: Technology Status and Application Development. In *ESSCIRC 2008 - 34th European Solid-State Circuits Conference*; 2008.

(2) Arias, A. C.; MacKenzie, J. D.; McCulloch, I.; Rivnay, J.; Salleo, A. Materials and Applications for Large Area Electronics: Solution-Based Approaches. *Chem. Rev.* **2010**, *110* (1), 3–24.

(3) Sekitani, T.; Nakajima, H.; Maeda, H.; Fukushima, T.; Aida, T.; Hata, K.; Someya, T. Stretchable Active-Matrix Organic Light-Emitting Diode Display Using Printable Elastic Conductors. *Nat. Mater.* **2009**, *8* (6), 494–499.

(4) Yang, J.; Vak, D.; Clark, N.; Subbiah, J.; Wong, W. W. H.; Jones, D. J.; Watkins, S. E.; Wilson, G. Organic Photovoltaic Modules Fabricated by an Industrial Gravure Printing Proofer. *Sol. Energy Mater. Sol. Cells* **2013**, *109*, 47–55.

(5) Lim, N.; Kim, J.; Lee, S.; Kim, N.; Cho, G. Screen Printed Resonant Tags for Electronic Article Surveillance Tags. *IEEE Trans. Adv. Packag.* **2009**, *32* (1), 72–76.

(6) Subramanian, V.; Frechet, J. M. J.; Chang, P. C.; Huang, D. C.; Lee, J. B.; Molesa, S. E.; Murphy, A. R.; Redinger, D. R.; Volkman, S. K. Progress Toward Development of All-Printed RFID Tags: Materials, Processes, and Devices. *Proc. IEEE* **2005**, *93* (7), 1330–1338.

(7) Grau, G.; Cen, J.; Kang, H.; Kitsomboonloha, R.; Scheideler, W. J.; Subramanian, V. Gravure-Printed Electronics: Recent Progress in Tooling Development, Understanding of Printing Physics, and Realization of Printed Devices. *Flexible and Printed Electronics* **2016**, *1* (2), 023002.

(8) Kitsomboonloha, R.; Morris, S. J. S.; Rong, X.; Subramanian, V. Femtoliter-Scale Patterning by High-Speed, Highly Scaled Inverse Gravure Printing. *Langmuir* **2012**, *28* (48), 16711–16723.

(9) Hennig, G.; Selbmann, K.-H.; Brockelt, A. Laser Engraving in Gravure Industry. In *Workshop on Laser Applications in Europe*; 2005.

(10) Sung, D.; de la Fuente Vornbrock, A.; Subramanian, V. Scaling and Optimization of Gravure-Printed Silver Nanoparticle Lines for Printed Electronics. *IEEE Trans. Compon. Packag. Technol.* **2010**, *33* (1), 105–114.

(11) Grau, G.; Kitsomboonloha, R.; Subramanian, V. Fabrication of a High-Resolution Roll for Gravure Printing of 2μm Features. In *Organic Field-Effect Transistors XIV; and Organic Sensors and Bioelectronics VIII*; 2015.

(12) Cen, J.; Kitsomboonloha, R.; Subramanian, V. Cell Filling in Gravure Printing for Printed Electronics. *Langmuir* **2014**, *30* (45), 13716–13726.

(13) Oliver, J. F.; Huh, C.; Mason, S. G. Resistance to Spreading of Liquids by Sharp Edges. *J. Colloid Interface Sci.* **1977**, *59* (3), 568–581.

(14) Bankoff, S. G. Entrapment of Gas in the Spreading of a Liquid over a Rough Surface. *AIChE J.* **1958**, *4* (1), 24–26.